Comparison of Numerical Simulation with Experimental Measurement of Temperature Field and Welding Deformation in Different Welding Sequences of Welding T-Joint

Manh Khang BUI [1, 2], Pham Hai Duong TRAN [1, 2], Van Hong Phuc NGUYEN [1, 2], Tran Vy Thao PHAN [1, 2], Kha Quoc LE [1, 2], Minh Tuan PHAM [1, 2], Tri Cong PHUNG [1, 2 *]

[1] *Faculty of Mechanical Engineering, Ho Chi Minh University of Technology (HCMUT), 268 Ly Thuong Kiet Street, District 10, Ho Chi Minh City, Vietnam*
[2] *Vietnam National University Ho Chi Minh City, Linh Trung Ward, Thu Duc City, Ho Chi Minh City, Vietnam*

http://doi.org/10.5755/j02.ms.38417

Received 9 August 2024; accepted 14 November 2024

The estimation of temperature field and welding deformation plays an important role in welding technology. The accuracy of the numerical simulation will reduce the cost of experimental measurement. This paper suggests the numerical simulation of the temperature field and welding deformation of the welding fillet joint, or welding T-joint, in different welding sequences. The first contribution of this paper is proposing the numerical model to simulate the heat transfer between the metal plates and the thermocouple sensor. The second contribution is that the paper shows the mechanical deformation in many welding sequences and concludes which welding sequence can give the smallest deformation. The proposed numerical model is verified by the experimental results.
Keywords: numerical simulation, experimental measurement, temperature field, welding deformation, fillet joint welding.

1. INTRODUCTION

Welding stands as one of the fundamental processes in modern manufacturing and construction, serving as the backbone for joining metallic components efficiently and securely. Automatic welding using robots has become popular in factories and companies. One of the problems in welding processes is that the engineers need to test and verify the welding lines, also several welding parameters before doing the real manufacturing. Achieving good-quality welding is the utmost priority in many industries. Therefore, understanding how welding parameters affect the quality of weldment continues to hold significant value in the modern era. One viable solution is estimating the parameters of the temperature field and mechanical properties by numerical simulation. Specifically, the accuracy of the numerical simulation is guaranteed to reduce the cost of the experimental measurements.

To overcome these difficulties, several experiments were conducted to build a numerical model that precisely describes the thermal properties and mechanical properties of the welding processes. There exists a multitude of researches about modelling the welding process by numerical methods and verifying the simulation results with the experimental measurements. Atul et al. [1] carried out a coupled Eulerian-Lagrangian model to investigate the influence of peak temperature in the stirred zone and axial force on defect formation during friction stir welding. This study enhances the understanding of the thermophysical interaction between the tool and the workpiece. Jianfeng et al. [2] constructed a new type of deflection heat source to simulate the welding temperature field to understand the asymmetric heat transfer distribution of dissimilar steel under the action of the external transverse magnetic field. Karpagaraj et al. [3] focused on the simulation of the GTA welding process and the simulation of the tensile and cupping test. Pardeep et al. [4] conducted both experimental and numerical analyses for the friction stir welding and plasma-assisted friction stir welding of dissimilar steels such as DH36 shipbuilding steel and AISI 1008 steel. Ilija et al. [5] analysed the problem of friction stir welding (FSW) technology by carrying out a numerical simulation of process welding FSW proceeding on the example of Aluminium Alloy (AA 2219) using the ANSYS Mechanical ADPL (Transient Thermal) software package. Zhuanni et al. [6] employed a coupled model, including macroscopic finite element and microscopic cellular automata with interpolation, to investigate the temperature field, thermal cycles, solidification parameters, and microstructure evolution under varied process parameters.

Due to its simplicity, fillet welding is commonly used in different industry sectors, including automotive, aerospace, shipbuilding, and structural engineering. Fillet welding or T-joint welding plays an important role in manufacturing. There are several research about building a numerical model that precisely describes the thermal properties and mechanical properties of the welding processes of T-joint. Dean et al. [7] developed a 3-D thermal elastic plastic finite element computational procedure to precisely predict welding deformation in the fillet-welded joints. Nima et al. [8] investigated the demands generated in the panel zone of welded steel built-up box columns with fillet and complete joint penetration (CJP) groove welds,

* Corresponding author: T.C. Phung
E-mail: *ptcong@hcmut.edu.vn*

which are mainly used as columns in steel moment-resisting frames. İlker et al. [9] employed the finite element (FE) method to evaluate residual stresses and angular distortions of fillet welded T-joints with an experimental validation. Rabih et al. [10] presented the finite element modelling of a two-seam welding process for a T-joint with a V chamfer preparation to predict the deformations, distortions, and residual stresses resulting from the welding of the plates. Raffaele et al. [11] reported an investigation of the welding process to make a dissimilar T-joint through advanced finite element (FE) modelling and a dedicated laboratory test through a Shielded Metal Arc Welding. Chungui et al. [12] established a three-dimensional thermomechanical coupled model of the Stationary Shoulder Friction Stir Welding process to simulate and analyse the temperature field and material flow. Minghui et al. [13] proposed a model to deeply investigate the tensile properties and fracture behaviours that are obtained by tensile tests of welded joints under different welding currents of Tungsten Inert Gas Welding (TIGW).

However, the above research did not mention the effect of the welding sequences on the quality of the welding joint. The welding deformation becomes large in a long welding line. Thus, it is necessary to divide this welding line into several smaller segments to alleviate the deformation. Additionally, the welding sequences of these lines will affect the welding deformation. Despite the significance of this problem, there is limited research presented regarding this problem. Mehran et al. [14] developed a computational approach based on the finite element (FE) method to efficiently predict welding deformations and residual stresses of fillet welded T-joints made of high strength steel (HSS), S700. using different welding sequences and external constraints. Zhongzhao et al. [15] simulated and analysed the welding process of fillet joints employing four different application sequences with the double ellipsoidal heat source model. The above research exclusively concentrated on simulation results and did not take the consideration of which is the best welding sequence into account.

This paper presents the numerical simulation of the temperature field and welding deformation of the welding fillet joint in different welding sequences. The primary contribution of this paper lies in the development of the numerical model that effectively simulates the heat transfer between the metal plates and the thermocouple. In prior research conducted, the sensor element of the thermocouple sensor is in the tip of the sensor, a design choice that this study seeks to modify to overcome the technological disadvantages of the experiment environment. Thus, the sensor can measure directly the temperature of the metal plate. In this research, the sensor element is positioned approximately 1.5 millimetres away from the tip of the sensor. The heat transfer between the metal plate and the thermocouple sensor needs to be considered. Our temperature simulation results illustrate a high degree of accuracy, as evidenced by Pearson's correlation coefficients exceeding 0.95. The second contribution is that the paper shows the mechanical deformation in many welding sequences and concludes which welding sequence can give the smallest deformation. By using the collective utility (CU) method, a sequence is identified with the smallest deformation index, corresponding to the highest CU value of approximately 0.893. The proposed numerical model is verified by experimental results.

The content of the paper can be presented in four sections. The first section presents the introduction of the paper and the contribution of the paper. Section 2 describes the proposed method and experimental setup. The third section shows the comparison between the 3D simulation and experimental results. Section 4 shows the conclusion.

2. EXPERIMENTAL DETAILS AND PROPOSED METHODS

This research proposes the numerical simulation model of temperature field and welding deformation of the fillet joint welding in different welding sequences. These simulation results are verified by experimental results.

2.1. Experimental setup

The experiment specimen consists of 2 plates of structural steel SS400 which are tacked and welded together manually. The dimensions of the flange are $150 \times 120 \times 6$ mm and that of the web is $150 \times 60 \times 6$ mm, the experimental model is shown in Fig. 1. Table 1 presents the chemical components.

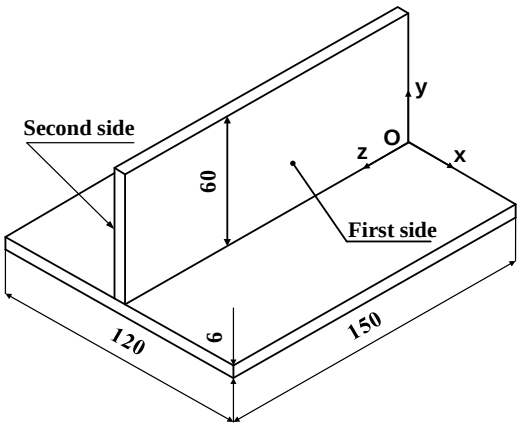

a

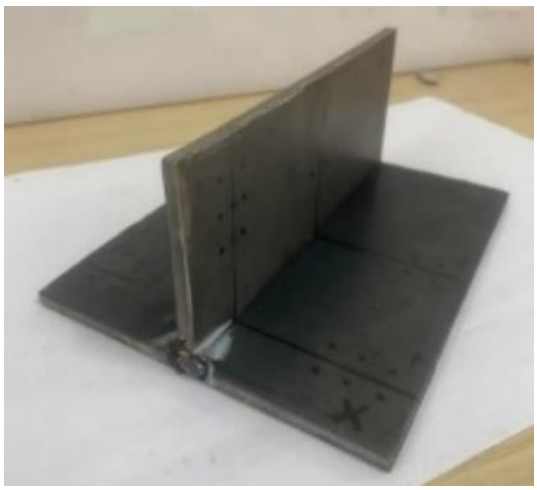

b

Fig. 1. The welding experimental model: a – specimen's dimensions and coordinates; b – real experiment specimen

Table 1. Chemical components of SS400 steel plate, %

Material	C	Si	Mn	Ni	Cr	P	S
SS400	0.11 – 0.18	0.12 – 0.17	0.4 – 0.57	0.03	0.02	0.02	0.03

To match the simulation with the experiment, the workpieces are elevated at 4 corners as shown in Fig. 2 and are constrained with clamps at the corresponding points. In this experiment, the forehand welding technique is employed, and the process is carried out by the robot Motoman UP6 with the welding angle described in Fig. 3 and welding parameters in Table 2. The angle between the welding plane and the x axis is 45°, and the angle between the torch and the in-plane perpendicular axis is 10°.

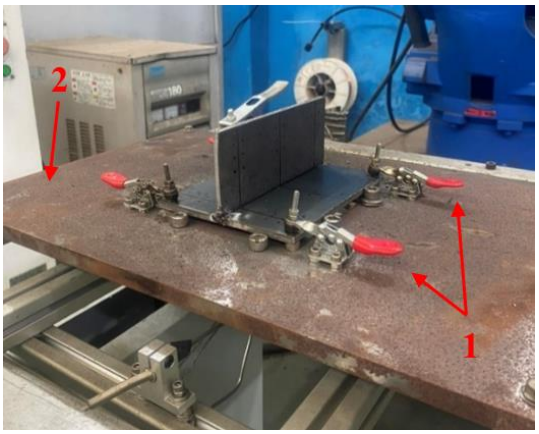

a

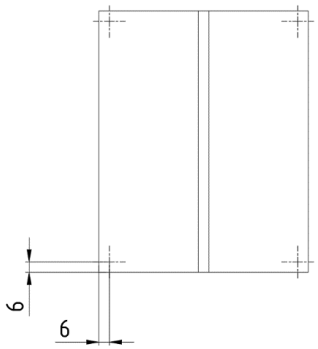

b

Fig. 2. a – welding table to clamp the fillet joint: 1 – clamp, 2 – welding table; b – the 4 clamping position on the flange

Table 2. Welding parameters

Current	Voltage	Travel speed	Distance from tip to workpiece	Protective gas
160 A	25 V	40 cm/min	5 mm	100 % CO_2

Temperature is measured under the flange surface with 4 K-type thermocouples and Fig. 3 shows the measured positions. The four thermocouples are secured by shaft holders as in Fig. 4 and they were bent to make sure they contact with the surface of the flange. The overall setup is as in Fig. 5.

The deformation of the flange and the web includes the vertical deformation of the flange and the angle distortion of the web shown in Fig. 6. These deformations are calculated from the straightness of 4 lines on the bottom surface of the flange shown in Fig. 7 a and the angular distortion α between the flange and the web, shown in Fig. 7 b.

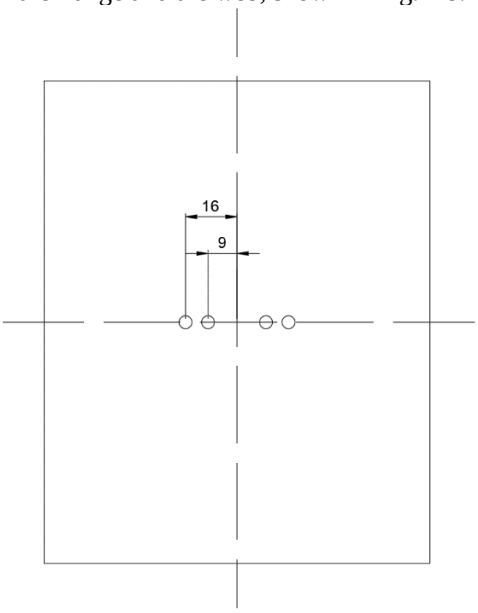

a

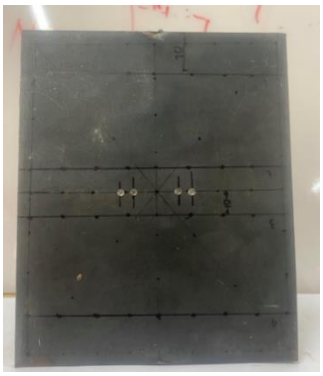

b

Fig. 3. Temperature measuring points: a – positions relative to the center line; b – drilled halfway to increase the contact area

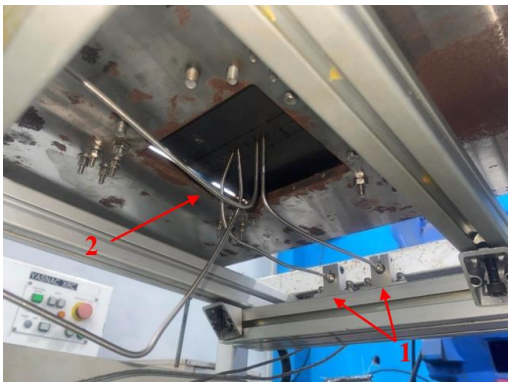

Fig. 4. Thermocouples placement: each was held with a shaft holder and bent to contact with the measured area: 1 – shaft holder; 2 – thermocouples

2.2. The 3D numerical model

The distribution of temperature fields and deformations were investigated using the finite element (FE) method. Since the displacements caused by welding are negligible in

comparison with the movement of the welding torch, thermal and mechanical analysis are performed separately.

Fig. 5. The overall setup: welding system with the 6DOF robot arm and welding table

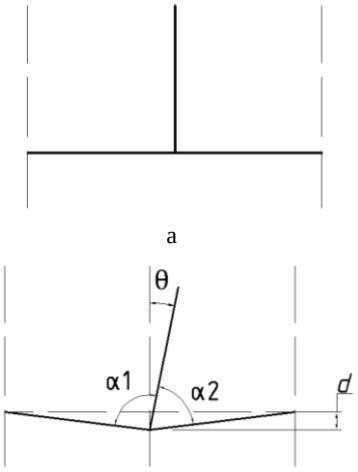

a

b

Fig. 6. a – before welding; b – after welding: α and the deviation d will be measured which then will be used to calculate θ

First, the heat conduction equation is solved to obtain the temperature field. Then the results from the transient heat analysis are fed into the mechanical simulation for the stress and strain fields.

The 3D numerical model includes 3 parts: the workpiece, the weldments, and the thermocouples. The thermo-mechanical properties are a combination of values by Deng et al. [16] and Jeyakumar et al. [17]. Artificially increased thermal conductivity is adopted when the temperature reaches above the melting point to avoid the unusually high weld pool temperature and imitate the flow of molten metal.

The first term on the right-hand side of Eq. 1 is convective heat loss, the second one is radiation heat loss. Heat losses due to convection and radiation are considered in a convenient format as:

$$q_n = h_c(T - T_{sur}) + \varepsilon\sigma(T^4 - T_{sur}^4) = h_{eff}(T - T_{sur}) \quad (1)$$

where h_c is the heat transfer coefficient, σ is the Stephan-Bolzmann's constant, ε is the emissivity factor, T is ambient temperature and T_{sur} is surface temperature.

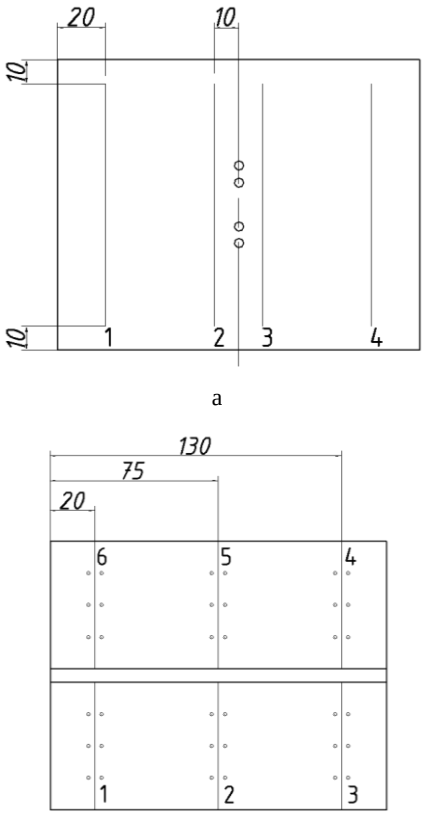

a

b

Fig. 7. a – lines for straightness measurement on the bottom surface of the flange; b – points for local plane approximation on the flange surface and the same for the web surface, in total measuring 3 angles on each side

The effective heat transfer coefficient is a combination of the convection and radiation coefficients.

$$h_{eff} = hc + \varepsilon\sigma(T^3 + T^2T_{sur} + TT_{sur}^2 + T_{sur}^3. \quad (2)$$

The thermal properties and mechanical properties are shown in Fig. 8 and Fig. 9 respectively.

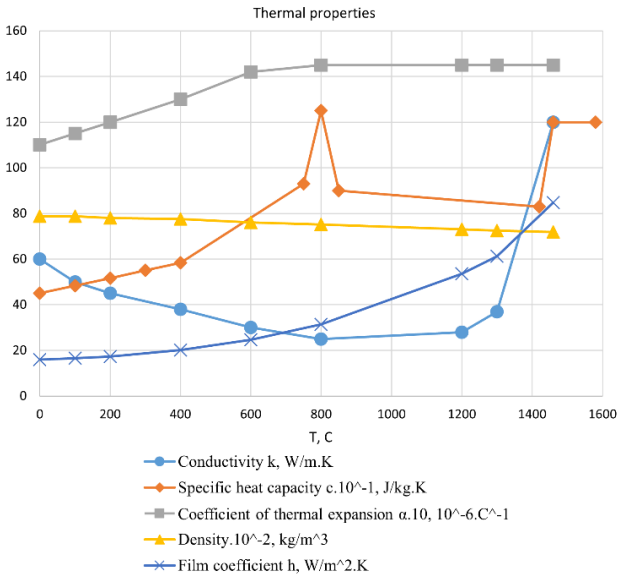

Fig. 8. Thermal properties of the SS400 steel plate [16, 17]

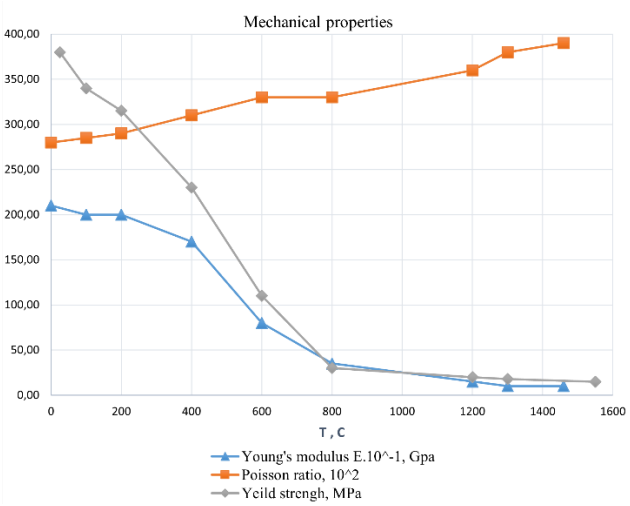

Fig. 9. Mechanical properties of the SS400 steel plate [16, 17]

In the thermal simulation, the time between two welding processes is set to 11 seconds, the total time of the welding process is 45 seconds, then the duration of the cooling step is 1000 seconds to allow the model to reduce its temperature naturally. The environmental temperature is set to 36 °C according to the real temperature at the experimental location. DC3D8, an 8-node linear heat transfer brick, is used in this thermal process. To balance the computing time and the accuracy of the simulation, a mesh grid was designed with a coarse grid away from the heat source and a fine grid along the heat source (Fig. 10). The total number of nodes is about 23000 and the total number of elements is about 19000.

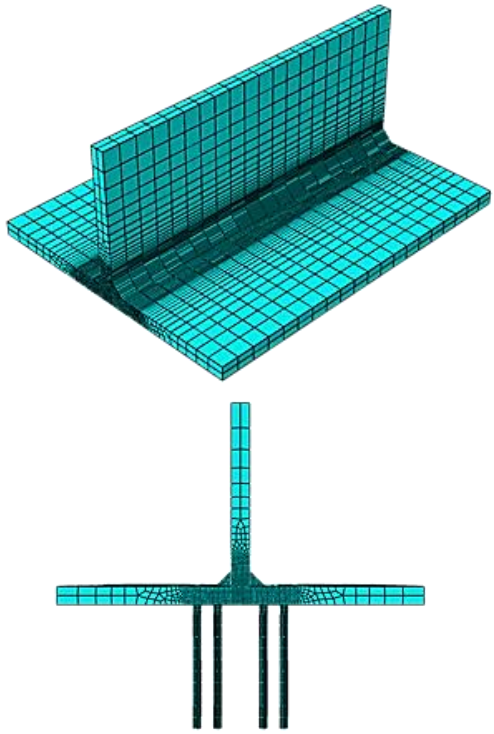

Fig. 10. The 3D FE model

The total heat input is calculated as:

$$Q = \eta . U . I, \tag{3}$$

where η is the heat efficiency of the GMAW method and is assumed to be 0.75 [18]; U is the welding voltage; I is the welding current.

The volumetric heat source in Fig. 11 using Goldak's double ellipsoid model [19], for butt-weld joint with Mokrov's modifications [20]. To apply to the T-joint welding, a coordinate transformation is needed for each side. The first side is first rotated around the z-axis at an angle equal to the welding angle $\theta = 45°$. For the second side, the global coordinate is first translated at a distance t = 6 mm to the opposite side and then rotated at the same angle. The front and rear heat input are calculated using the following equation:

$$q_f(x,y,z,t) = \frac{4\sqrt{2}.Q.f_i}{a.b.c_i.m.\pi\sqrt{\pi}} . e^{-2\left(\frac{X^2}{a^2}+\frac{Y^2}{b^2}+\frac{Z^2}{c_i{}^2}\right)}, \text{W/m}^3 \tag{4}$$

where m = 0.691368; a,b,c_i are the radii of the ellipses. X,Y and Z are the transformed coordinates; f_i is the energy fraction of the front and rear of the ellipsoid distribution; f_i and c_i are equal to f_f and c_f for the front half and are equal to f_r and c_r for the back half. Z is calculated as:

$$Z = v.(t - \tau), \tag{5}$$

where v is the welding speed; t is time and τ is the time offset for different starting points. The transformation matrices are as follows:

For the first side:

$$\begin{bmatrix} X \\ Y \\ Z \end{bmatrix} = \begin{bmatrix} \cos(\pi/4) & -\sin(\pi/4) & 0 \\ \sin(\pi/4) & \cos(\pi/4) & 0 \\ 0 & 0 & 1 \end{bmatrix} . \begin{bmatrix} x \\ y \\ z \end{bmatrix}, \text{mm} \tag{6}$$

For the second side:

$$\begin{bmatrix} X \\ Y \\ Z \end{bmatrix} = \begin{bmatrix} \cos(\pi/4) & \sin(\pi/4) & 0 \\ -\sin(\pi/4) & \cos(\pi/4) & 0 \\ 0 & 0 & 1 \end{bmatrix} . \begin{bmatrix} x+t \\ y \\ z \end{bmatrix}, \text{mm} \tag{7}$$

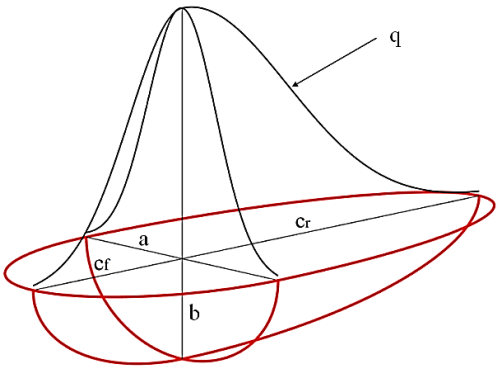

Fig. 11. The volumetric heat source model

The same model in thermal analysis is imported to the mechanical analysis, with the modification of element type and the boundary condition, the temperature field from the thermal analysis is used as a predefined field of the mechanical analysis. The C3D8I element type is used to simulate the stress-strain field. The boundary conditions (in Fig. 12) are then added correspondingly to the experimental setup. The thermocouples are always in contact with the plate.

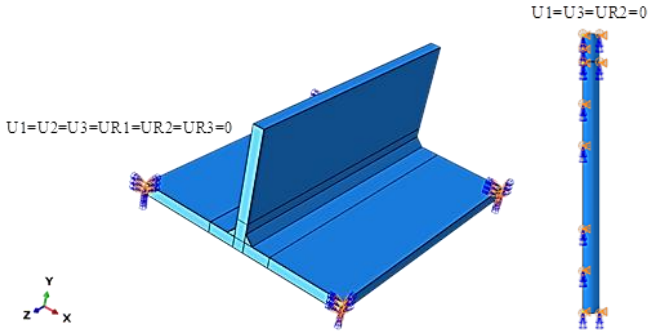

a b

Fig. 12. The mechanical constraints: a – the T-joint plates; b – the thermocouples

2.3. Welding process

The heating and cooling cycle of the welding path causes non-uniform expansion and contraction of the weld and the base material. Since the distortion in the range of 1 – 1.6 mm is very large, this paper proposes new welding sequences to reduce deformation. As can be seen from Fig. 13, the distortion becomes larger at the end of the welding line and the longer the welding line the larger the distortion; this suggests that the welding line should be split up into many small welding lines.

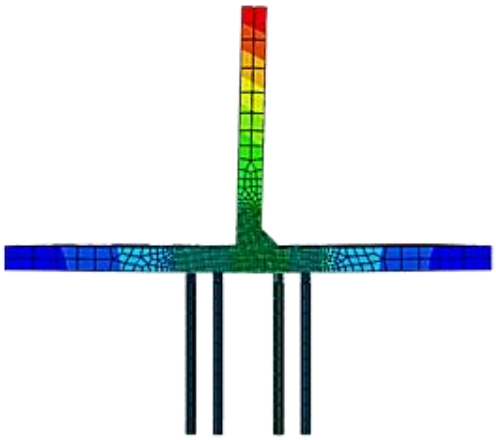

a

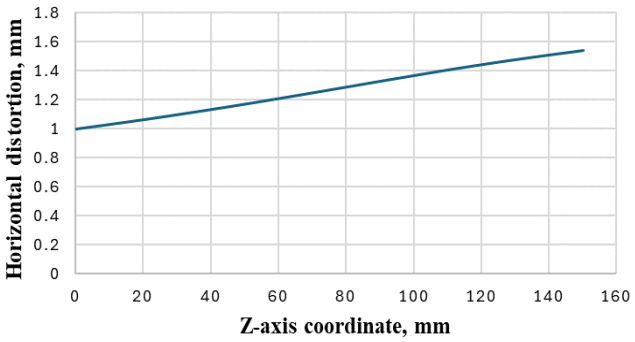

b

Fig. 13. a – the deformation of 1-side welding; b – hrizontal distortion distribution along the welding line

3. RESULTS AND DISCUSSION

3.1. Comparison between experimental results and 3D simulation results of temperature field

After calibrating the experimental results with, numerical methods, the graphs of the experiments and the graphs of the 3D simulations produced similar temperature characteristics (from Fig. 14 to Fig. 21). The first and the second sequences demonstrate perspicuous peaks. However, regarding the remaining sequences, the decreases in temperature between peaks are obscure. Generally, the temperature in the experiments escalates uniformly.

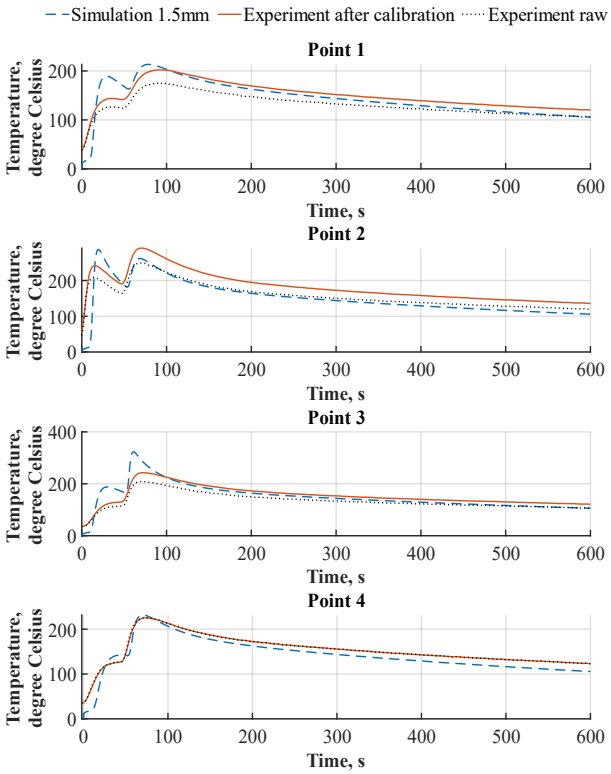

Fig. 14. Comparison between experimental result and simulation result of sequence no.1

Due to the insulation layer of the thermocouples, the temperature matching is stagnant for the first two peaks. The initial heat loss has the purpose of warming up those layers. From the initial sequence to the last sequence, the temperature in both simulation and experiment delivers a downward trend. Regarding the maximum temperature that comes on each graph, there is a resemblance between the range of the simulations and the experiments. Nonetheless, a variation of their lowest temperature exists, except that the gap in every case is stable around 50 degrees. Besides the similitude, it is perceptible that samples 2, 5, and 6 comprehend a more pronounced disparity between computerized and real-life outcomes. Accumulating all the evidence, the final results calibrated by mathematics methods are satisfactory.

To accentuate the similarity between the experimental results and the simulation results, Pearson's correlation coefficient [22] is used (Table 3). In each sequence, the results of thermocouple number 4 are selected to represent the calculation of the correlation coefficients. It is

indisputable that the mathematical model is effective since the coefficients computed by calibrated results are higher than those computed by the raw data.

Table 3. Pearson's r correlation coefficients of simulation vs. raw and calibrated experimental data

Sequence	Raw experiment vs. Simulation	Calibrated experiment vs. Simulation
1	0.9691	0.9750
2	0.9513	0.9556
3	0.9796	0.9786
4	0.9827	0.9835
5	0.9859	0.9888
6	0.9585	0.9598
7	0.9900	0.9888
8	0.9844	0.9864

To exhibit the potency of the mathematical model, the means of errors between 3 types of data have been analyzed. Using point 4 of each sequence, Table 4 discloses the differences in the accuracy of data.

Table 4. The means of errors of simulation vs. raw and calibrated experimental data

Sequence	Raw experiment vs. Simulation	Calibrated experiment vs. Simulation
1	26.6655	24.3311
2	33.7700	33.2704
3	24.4794	20.0200
4	20.6396	7.3742
5	8.3018	11.5386
6	13.4164	13.2147
7	21.0435	8.9550
8	36.2220	15.0378

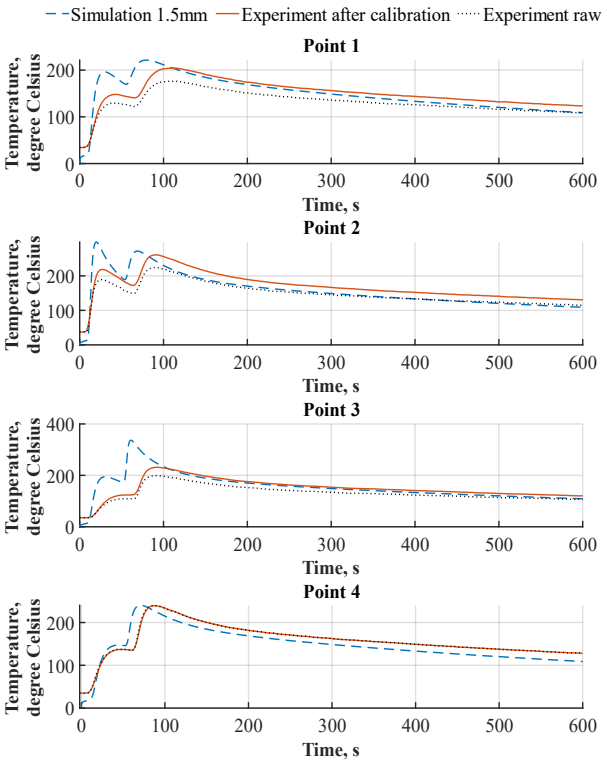

Fig. 15. Comparison between experimental result and simulation result of sequence no.2

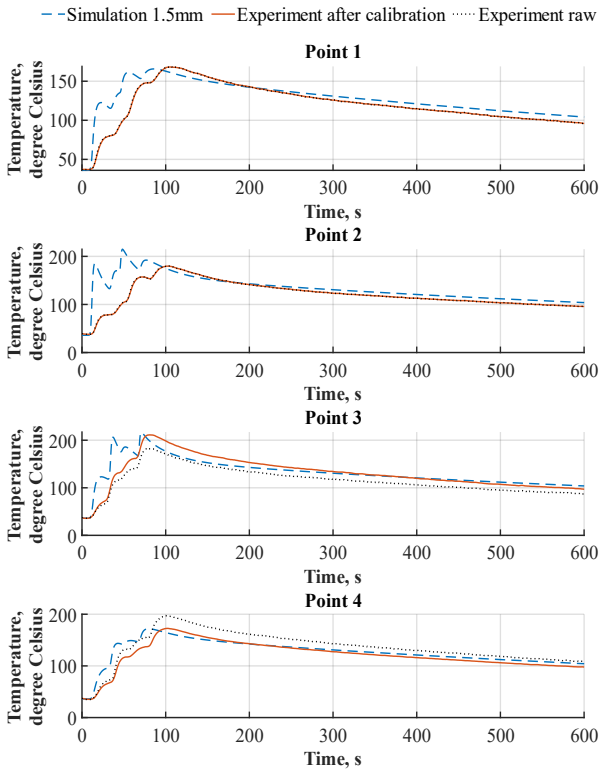

Fig. 16. Comparison between experimental result and simulation result of sequence no.3

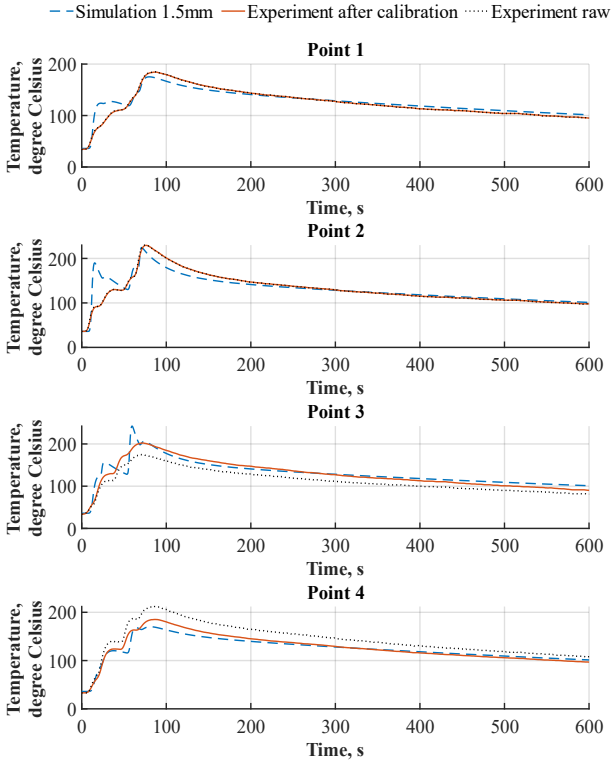

Fig. 17. Comparison between experimental result and simulation result of sequence no.4

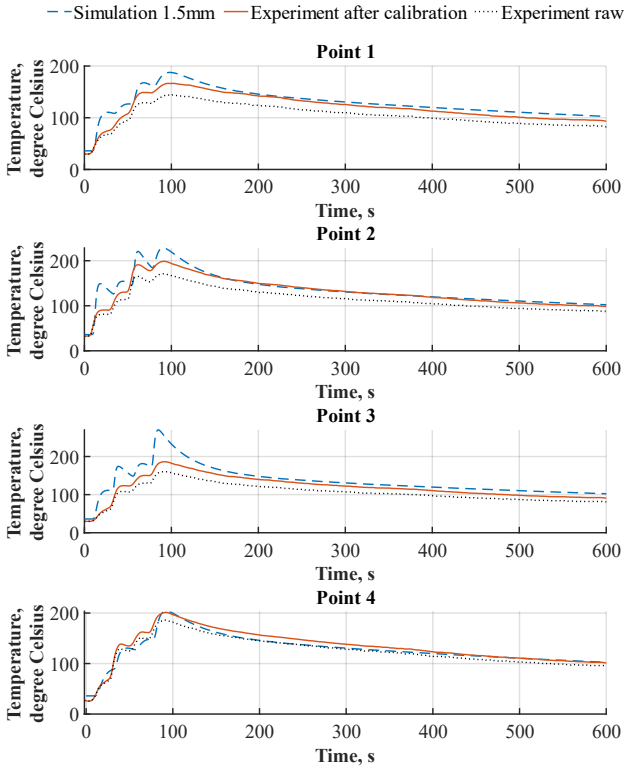

Fig. 18. Comparison between experimental result and simulation result of sequence no.5

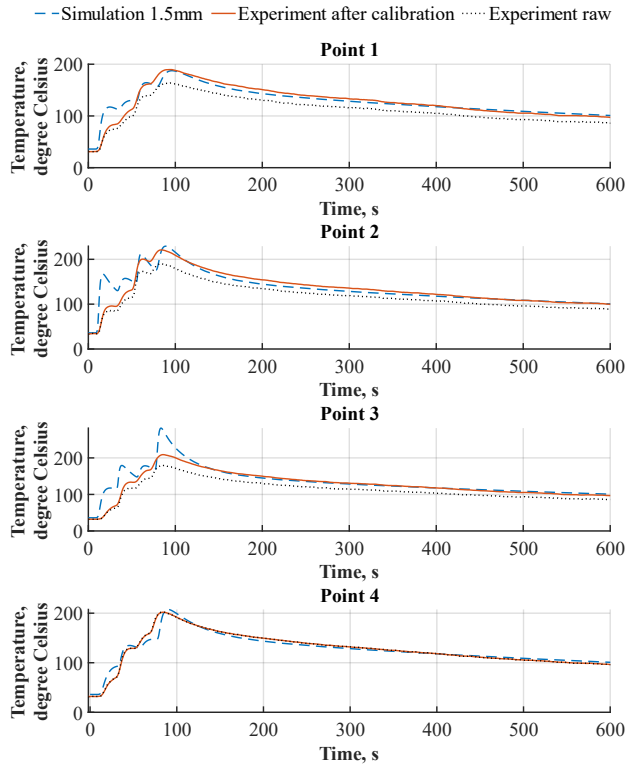

Fig. 19. Comparison between experimental result and simulation result of sequence no.6

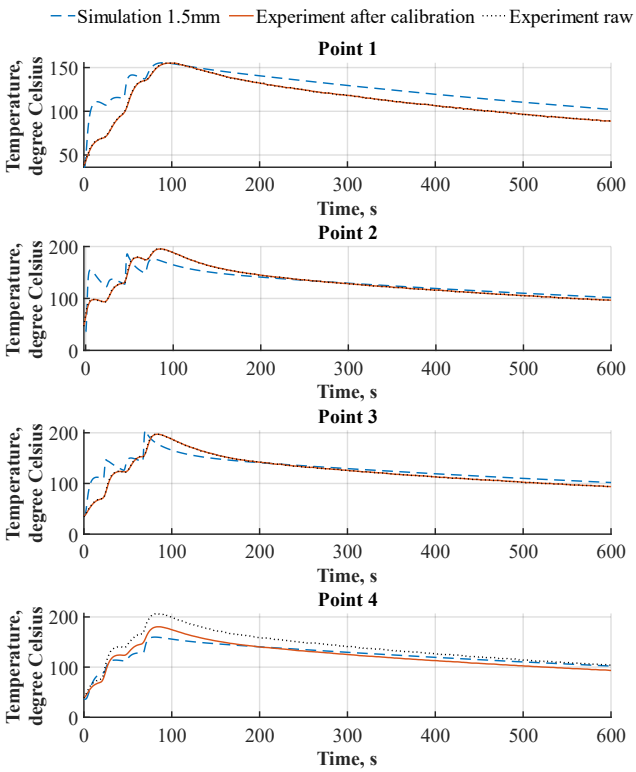

Fig. 20. Comparison between experimental result and simulation result of sequence no.7

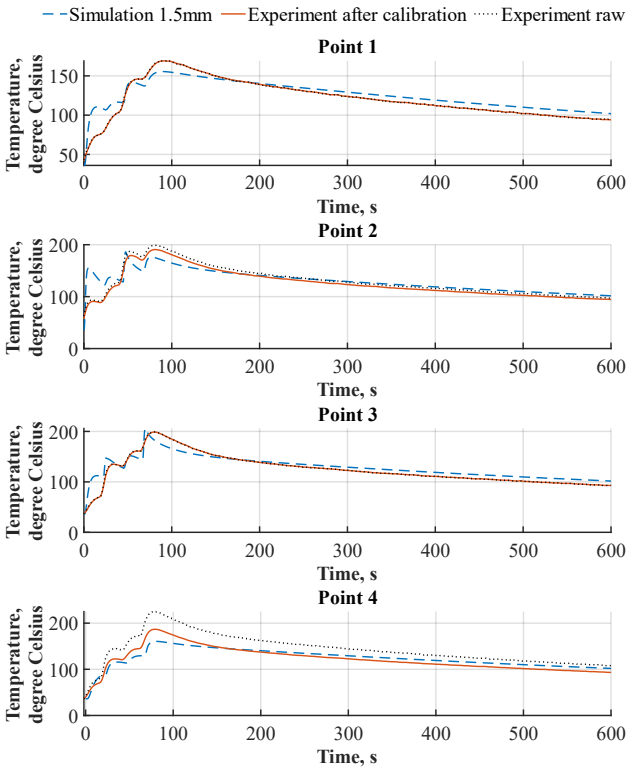

Fig. 21. Comparison between experimental result and simulation result of sequence no.8

From Fig. 22, the RMSE values of sequences 4, 5, 6, 7 and 8 are better than sequences 1, 2, 3. The RMSE remains below 60 degrees Celsius. Collectively, the experimental results exhibit a closer alignment with the simulation data in most sequences. Moreover, the experimental results must be adjusted to account for the time response characteristics of the thermocouples. The simulation model also requires considering all the heat transfer factors, for example, heat transfer through the thermocouples.

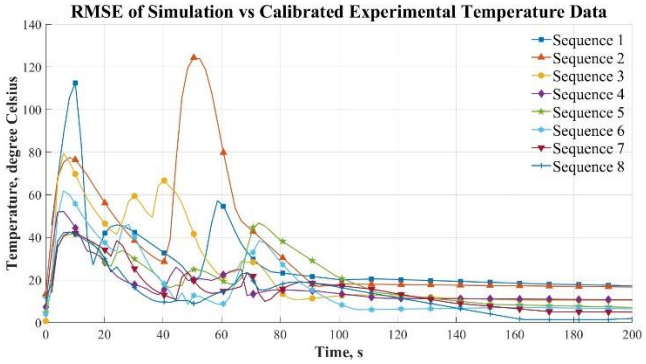

Fig. 22. Comparison between RMSE of calibrated experiment results and simulations of 8 sequences through time

3.2. Comparison between experimental results and 3D simulation results of welding deformation

The numerical-experimental vertical deformation graphs along the z-axis of the 8 welding sequences are shown in Fig. 23. Since all the models absorb the same amount of heat along the two sides of the plate, the deformation trend can be the same if they are seen on the opposite sides.

The maximum error between simulation and experiment is about 0.3 mm, however, in general, the trend of the deformation of both is quite similar.

The numerical-experimental angular distortion graphs along the z-axis of 8 welding sequences are shown in Fig. 24. There have been the differences between simulation and experiment, due to several reasons that will be mentioned below, however, the value differences are quite small and the differences of the shape of the two lines in each graph can be ignored so that they can be seen to be similar in the trend of the deformation.

According to the graphs in Fig. 23 and Fig. 24, the vertical deformation and horizontal distortion of T-joint welding between the simulation and experiment is different because the experiment has many disturbances which affect the deformation of the steel plate such as non-ideal ambient temperature affecting the heat dissipation ability of the welded plate, initial deviation of the steel plate, trustworthiness of the steel supplier, etc. However, deformation trends are quite similar, so it can be concluded that the simulation model can be trusted to predict the deformation tendency.

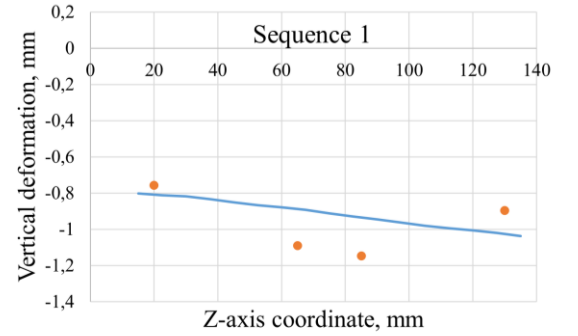

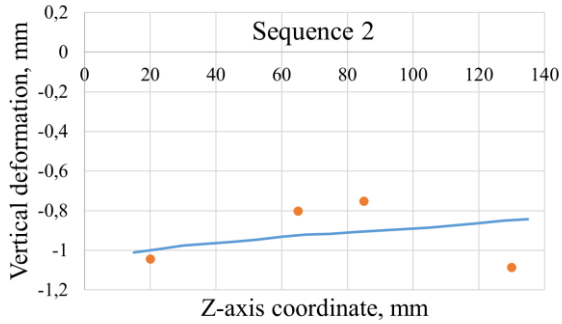

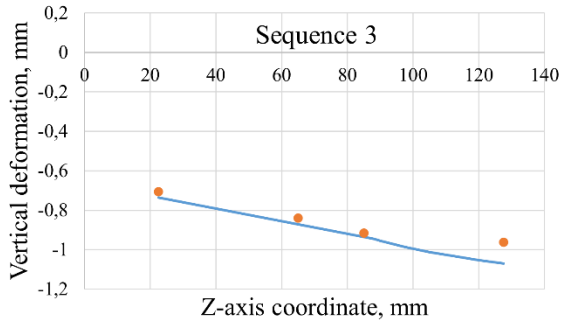

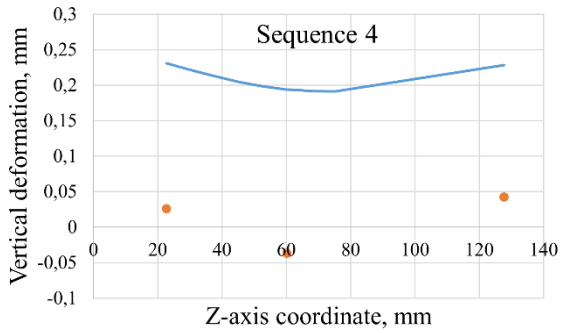

a

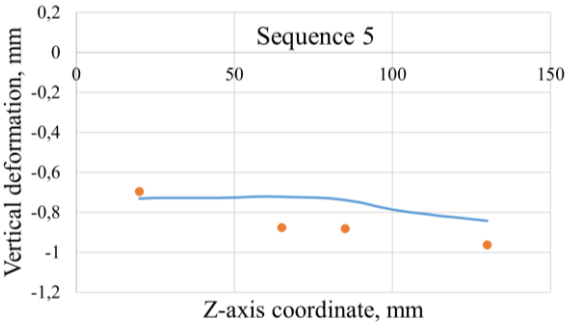

continued on next page

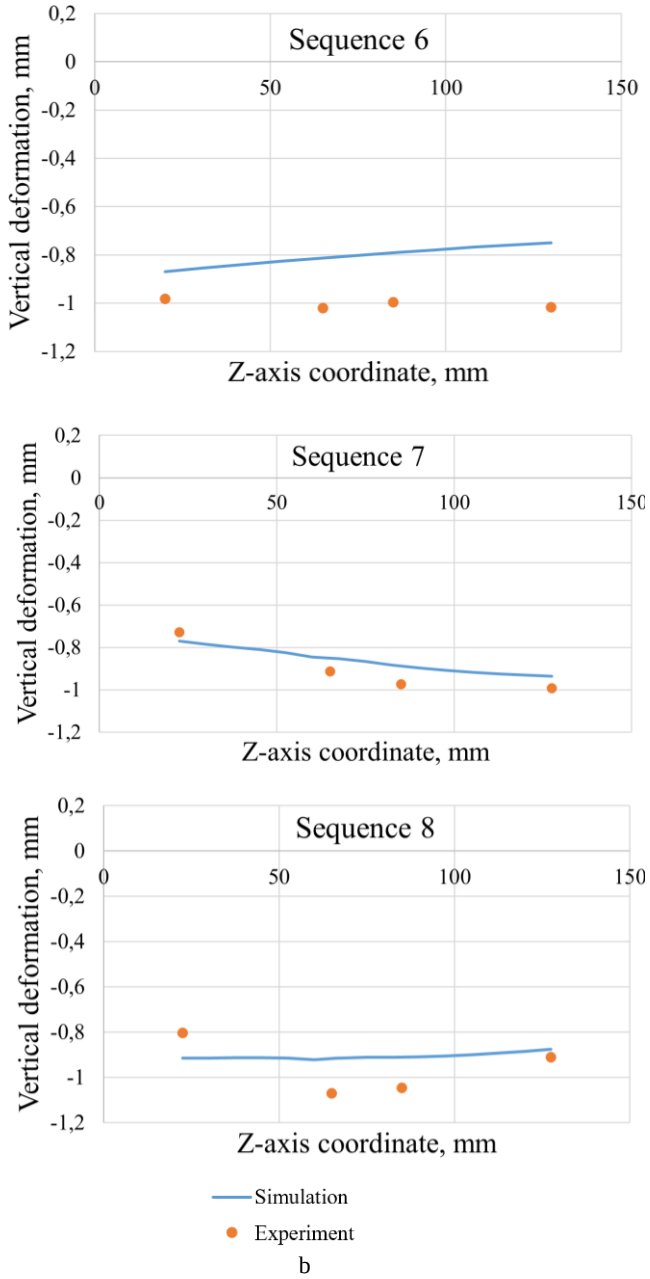

Fig. 23. Comparison between simulation and experiment results of the vertical deformation of the flange: a – from sequence 1 to sequence 4; b – from sequence 5 to sequence 8

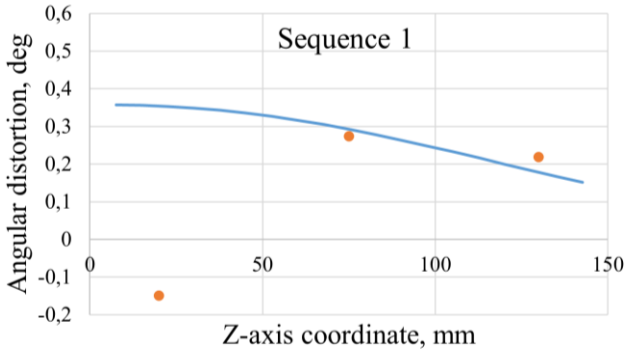

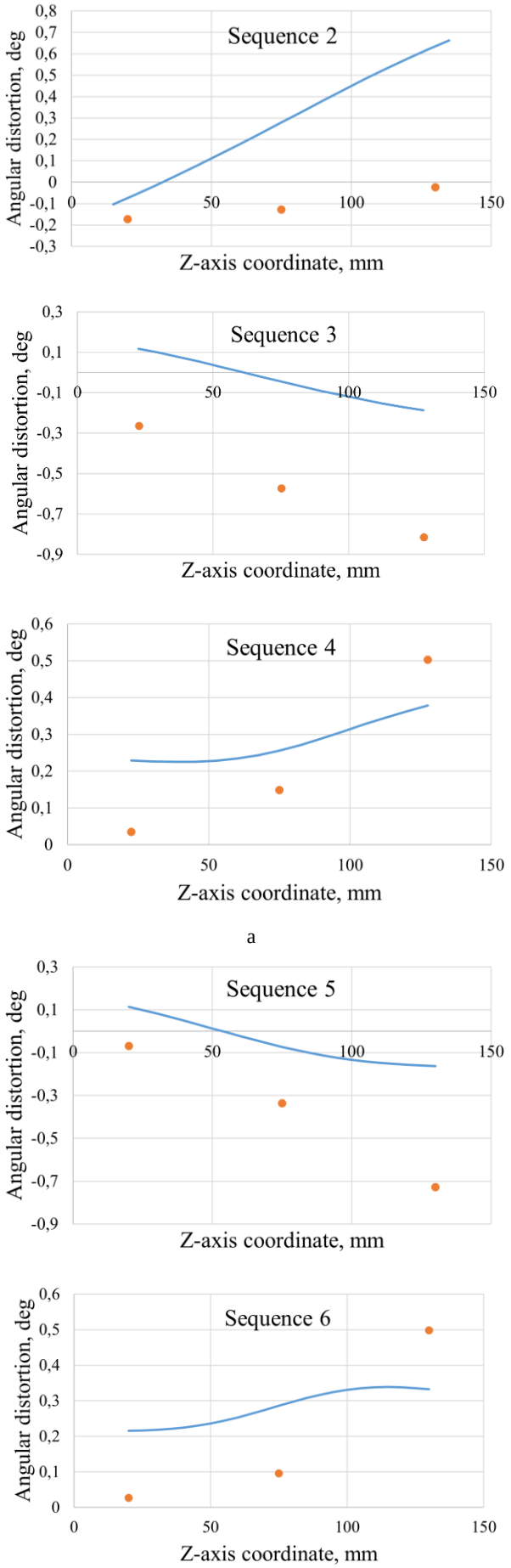

continued on next page

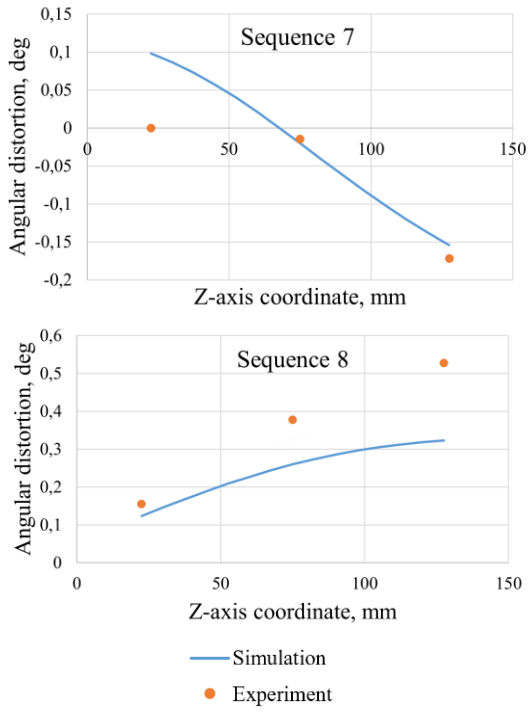

b

Fig. 24. Comparison between simulation and experiment results of the angular distortion of the web: a – from sequence 1 to sequence 4; b – from sequence 5 to sequence 8

3.3. Effect of welding sequences on the welding deformation

First, the effects of welding sequences on vertical displacement and angular distortions are judged separately. According to Table 5, sequences 4 and 5 are optimal in terms of vertical deformation.

Table 5. The average vertical deformation after welding (experimental result)

Sequence number	Vertical deformation, mm
1	0.9723
2	0.9216
3	0.8559
4	0.0351
5	0.8544
6	1,0041
7	0.9021
8	0.9570

According to Table 6, sequences 2 and 7 produce the least angular distortion.

Table 6. The average angular distortion after welding (experimental result)

Sequence number	Angular distortion, deg
1	0.2141
2	0.1081
3	0.5515
4	0.2286
5	0.3778
6	0.2067
7	0.0621
8	0.3534

However, to be able to evaluate which welding sequence is better, both types of displacement need to be considered hand in hand. This article uses the collective utility (CU) method [23] to choose the best sequence for welding. First, a criteria table for each sequence is established.

Table 7. Criteria table for the experimental result

Sequence number	Criteria	
	Vertical deformation	Angular distortion
1	0.9723	0.2141
2	0.9216	0.1081
3	0.8559	0.5515
4	0.0351	0.2286
5	0.8544	0.3778
6	1.0041	0.2067
7	0.9021	0.0621
8	0.9570	0.3535
Weight	0.5	0.5

Then, the equation for the CU method is as follows: Transform from Z_{ij} to b_{ij}

$$b_{ij} = \frac{|z_{i\,max} - z_{ij}|}{|z_{i\,max} - z_{i\,min}|}, \quad (8)$$

whereas i is the number of rows; j is the number of columns; Z_{ij} is the initial value from Table 7.

$$CU_j = b_{ij} \times weight. \quad (9)$$

Table 8 after applying the transform equation.

Table 8. The experimental result after applying the transform

Sequence number	Criteria		CU
	Vertical deformation	Angular Distortion	
1	0.0328	0.6896	0.3612
2	0.0851	0.9061	0.4957
3	0.1529	0	0.0765
4	1	0.6598	**0.8299**
5	0.1545	0.3549	0.2547
6	0	0.7046	0.3523
7	0.1053	1	**0.5526**
8	0.0486	0.4047	0.2267
Weight	0.5	0.5	

It can be seen that sequence 4 has the smallest deformation index because it has the biggest CU number. It can be concluded that sequence 4 is the best sequence for welding according to actual measurement results.

The simulation result will also be judged the same way as the experimental result. Table 9 shows that sequence numbers 4 and 5 are the best choices for the welding process according to vertical deformation.

Table 9. The average vertical displacement after welding (simulation result)

Sequence number	Vertical deformation (mm)
1	0.9139
2	0.9200
3	0.9737
4	0.2066
5	0.7570
6	0.8047
7	0.8646
8	0.9071

Table 10. The average angular distortion after welding (simulation result)

Sequence number	Angular distortion, deg
1	0.2773
2	0.3005
3	0.0907
4	0.2766
5	0.0927
6	0.2815
7	0.0730
8	0.2455

Table 10 shows that the sequence number 3 and 7 are the better choice for the welding process according to angular distortion.

Table 11. Criteria table for the simulation result

Sequence number	Criteria	
	Straightness tolerance	Angular distortion
1	0.9139	0.2773
2	0.9200	0.3005
3	0.9737	0.0907
4	0.2066	0.2766
5	0.7570	0.0927
6	0.8047	0.2815
7	0.8646	0.0730
8	0.9071	0.2455
Weight	0.5	0.5

Table 12. Simulation result after apply the transform

Sequence number	Criteria		CU
	Straightness tolerance	Angular distortion	
1	0.0779	0.1019	0.0899
2	0.0699	0	0.0350
3	0	0.9223	0.4611
4	1	0.1051	**0.5525**
5	0.2824	0.9137	**0.5980**
6	0.2203	0.0836	0.1520
7	0.1421	1	**0.5710**
8	0.0868	0.2420	0.1644
Weight	0.5	0.5	

It can be seen from Table 11 and Table 12 that sequence 5 has the smallest deformation index because it has the biggest CU number. It can be concluded that sequence 5 is the best sequence for welding according to simulation measurement results.

From the experiment results, sequences 4 and 7 are the best. From the simulation results, sequences 5, 7, and 4 are the best sequence respectively. Both the experiment and simulation all agree that sequence 7 and sequence 4 are ones of the best sequences.

3.4. Discussion

Concerning thermal simulation, in [7, 14, 15], most of the research used Goldak's double ellipsoid heat source model to great success. This research uses and examines Mokrov's modifications [20] for said heat source for the fillet weld. Because of the way of using thermocouples, our research also includes the thermocouple model in the FE simulation. This paper expands on previous papers by showing the effect that the thermocouple insulating layer has on the final temperature reading when in direct contact with the steel plates.

The research conducted by Dean [7] has demonstrated that the deformation of the fillet-welded joint in simulation and experiment are similar. However, the heat conduction process in their research has only been analyzed in simulation, without verification through experiment. Derivatively, our research has computed similar simulation results, enhancing their approach with the comparison between the simulation results and the experimental results. Conspicuously, our temperature simulation was testified with empirical data before the measurement and the affirmation of the mechanical deformation.

In terms of deformations and the affecting factors, various conclusions were reached. Raffaele Sepe et al. [11] measured the displacement of each side of the T-joint plate using only 1 point on the mid-section furthest from the center. This paper proposes a different method that uses 4 lines on the bottom of the flange to calculate the straightness and measuring 3 angular distortions of the flange and the web on each side of each sequence. The results are compared with the corresponding simulation and can be concluded that the numerical simulation can predict the deformation tendency.

The deformation of the T-joint is investigated thoroughly with different welding sequences and mechanical boundary conditions by Mehran et al [14]. Two different welding sequences were experimented each with only 2 welding passes. It should be noted that the second welding pass only starts when the specimen has cooled down to room temperature. On the other hand, this paper focuses more on different welding sequences while simulating and experimenting with the welding procedure in a manufacturing manner, there is little resting time between each welding pass.

Zhongzhao [15] and Fu [21] both examined the effects of welding sequences on the distortion of the fillet weld though they only did so via numerical simulation without experimenting. This paper builds upon the previous works by experimentally examining the effects of 8 welding sequences on welding deformations and experimentally evaluating those welding sequences. Especially for Fu's paper, Sequence 1, 2, 3, and 5 in this paper correspond to sequences a, b, e, f in their paper. This research agrees with the fact that partitioning the weld line into smaller lines yields smaller angular distortion. Moreover, from sequences 3 to 8, starting from the middle of the joint produces less horizontal deformation than the block welding processes which start from 1 of the 2 ends of the T-joint.

4. CONCLUSIONS

In this paper, the thermos and mechanical numerical FE model was developed to predict the temperature field and deformations distribution of a fillet weld joint. Various welding sequences are also simulated and experimented with. The conclusions are as follows:

1. The 3D numerical model including the thermocouples can predict the temperature of consecutive weld passes if there's a large enough time interval between them.
2. The FE model can accurately predict the vertical deformations of the flange. However, regarding the

angular distortion of the web, due to imperfections in the prepared specimen, numerical simulation can only predict the deformation tendency.

3. The CU method can be employed to decide on the effectiveness of welding sequences. The Pearson r correlation method can also be used to evaluate the similarity between the simulated temperature distribution and experimental results.
4. Surprisingly, in progressive welding for sequences 1 and 2, welding the 2nd pass in the same direction is better than welding in the opposite direction.
5. As expected, dividing the welding process into smaller lines reduces the distortions in general. Among them, sequences 4, 5, and 7 show the best result.

Acknowledgments

This research is funded by Vietnam National University HoChiMinh City (VNU-HCM) under grant number B2021-20-03. We acknowledge the support of time and facilities from Ho Chi Minh City University of Technology (HCMUT), VNU-HCM for this study.

REFERENCES

1. **Atul, K.C., Rahul, J.** Influence of Stir Zone Temperature and Axial Force on Defect Formation and Their Effect on Weld Efficiency During Friction Stir Welding of AA1100: A Simulation and Experimental Investigation *Material Today Communications* 37 (107413) 2023: pp. 1 – 14. https://doi.org/10.1016/j.mtcomm.2023.107413
2. **Jianfeng, Y., Hao, Z., Chang, X., Wei, Z., Wenji, L.** Temperature Field Simulation and Asymmetric Heat Transfer Distribution of Dissimilar Steel Welded with External Transverse Magnetic Field *Material Today Communications* 37 (107141) 2023: pp. 1 – 12. https://doi.org/10.1016/j.mtcomm.2023.107141
3. **Karpagaraj, A.,Kumar, N.R., Sankaranarayanasamy, K., Shanmugam, N.S., Muralimohan, C**. Simulation and Experimental Studies on Arc Efficiency and Mechanical Characterization for GTA-Welded Ti–6Al–4V Sheets *Arabian Journal for Science and Engineering Research Article – Mechanical Engineering* 45 2020: pp. 9639 – 9650. https://doi.org/10.1007/s13369-020-04876-x
4. **Pardeep, P., Avinish, T., Pankaj, B., Rao, A.G**. Plasma-Assisted Hybrid Dissimilar Friction Stir Welding for Joining of DH36 Steel and AISI 1008 Steel: Thermal Modelling and Experimental Analysis *Arabian Journal for Science and Engineering Research Article-Mechanical Engineering* 46 2021: pp. 7929 – 7952. https://doi.org/10.1007/s13369-021-05574-y
5. **Ilija, K., Mirko, D., Goran, T., Stevan, M.** Influential Parameters and Numerical Simulation of Heat Generated in the Process of Friction Stir Welding *Materials Science (Medžiagotyra)* 22 (3) 2016: pp. 348 – 353. https://doi.org/10.5755/j01.ms.22.3.10022
6. **Zhuanni, G., Xiaohong, Z., Huizi, S., Yifan, L., Xiang, L., Zhiqiang, L., Leilei, W.** Mechanism of Columnar to Equiaxed to Lamellar Grain Transition during Wire-Laser Directed Energy Deposition 205 C Aluminum Alloy Utilizing a Coaxial Head: Numerical Simulation and Experiment *Journal of Materials Processing Technology* 322 (118208) 2023: pp. 1 – 15. https://doi.org/10.1016/j.jmatprotec.2023.118208
7. **Dean, D., Wei, L., Hidekazu, M.** Determination of Welding Deformation in Fillet-Welded Joint by Means of Numerical Simulation and Comparison with Experimental Measurements *Journal of Materials Processing Technology* 183 (2 – 3) 2007: pp. 219 – 225. https://doi.org/10.1016/j.jmatprotec.2006.10.013
8. **Nima, T., Seyed, R.M., Abazar, A., Mohammadjavad, H.** Experimental and Numerical Study on Weld Strengths of Built-Up Steel Box Columns *Journal of Constructional Steel Research* 213 (108362) 2024: pp. 1 – 15. https://doi.org/10.1016/j.jcsr.2023.108362
9. **İlker, E., Melike, S., Karasu, A.** Finite Element Simulation and Experimental Validation of Welding Distortion of Fillet Welded T-joints *Journal of Polytechnic* 25 (1) 2022: pp. 455 – 466. https://doi.org/10.2339/politeknik.881438
10. **Rabih, K.K., Henri, C., Ngan, V.L., Jacques, L., Marc, T.** Experimental and Finite Element Analysis of a T-Joint Welding *Journal of Mechanics Engineering and Automation* 2 2012: pp. 411 – 421.
11. **Raffaele, S., Venanzio, G, Alessandro, G., Alessandro, D.L.** FEM Simulation and Experimental Tests on the SMAW Welding of a Dissimilar T-Joint *Metals* 11 (7) 1016 2021: https://doi.org/10.3390/met11071016
12. **Chungui, W., Jun, D., Chunlin, D., Yunqiang, Z.** Numerical Simulation and Experimental Studied on Stationary Shoulder Friction Stir Welding of Aluminum Alloy T-Joint *Frontiers in Materials* 9 2022: pp. 1 – 8. https://doi.org/10.3389/fmats.2022.898929
13. **Minghui, P., Yuchao, L., Siyuan, S., Wenhe, L., Yan, X., Wencheng, T.** Tensile Behaviors and Mechanical Property Analyses of T-Welded Joint for Thin-Walled Parts in Consideration of Different TIG Welding Currents Using Multiple Damage Models and Fracture Criterions: Numerical Simulation and Experiment Validation *Materials* 16 (13) 2023: pp. 4864 – 4888. https://doi.org/10.3390/ma16134864
14. **Mehran, G., Antti, A., Joseph, A., Timo, B.** Welding-Induced Stresses and Distortion in High-Strength Steel T-Joints: Numerical and Experimental Study *Journal of Constructional Steel Research* 189 (107088) 2022: pp. 1 – 17. https://doi.org/10.1016/j.jcsr.2021.107088
15. **Zhongzhao, Y., Jianchun, L., Chuanlu, X., Shijie, Z.** Numerical Simulation of Welding Temperature Field, Stress Field, and Strain Field of Fillet Joint in Different Welding Sequence *Journal of Physics: Conference Series* 2541 (012003) 2023: pp. 1 – 9. https://doi.org/10.1088/1742-6596/2541/1/012003
16. **Deng, D., Murakawa, H.** Prediction of Welding Distortion and Residual Stress in a Thin Plate Butt-Welded Joint *Computational Materials Science* 43 (2) 2008: pp. 353 – 365. https://doi.org/10.1016/j.commatsci.2007.12.006
17. **Jeyakumar, M., Christopher, T.** Influence of Residual Stresses on Failure Pressure of Cylindrical Pressure Vessels *Chinese Journal of Aeronautics* 26.6 2013: pp. 1415 – 1421. https://doi.org/10.1016/j.cja.2013.07.025
18. **Jenney, C.L., O'Brien, A.** Welding Handbook: Welding Science And Technology. American Welding Society, 2001.
19. **Goldak, J., Chakravarti, A., Bibby, M.** A New Finite Element Model for Welding Heat Sources *Metallurgical Transactions B* 15 1984: pp. 299 – 305. https://doi.org/10.1007/BF02667333

20. **Mokrov, O., Simon, M., Schiebahn, A., Reisgen, U.** A Fine Modification of the Double Ellipsoid Heat Source *Mathematical Modelling of Weld Phenomena* 12 2019: pp. 39 – 50. https://doi.org/10.3217/978-3-85125-615-4-04
21. **Fu, G., Lourenço, M.I., Duan, M., Estefen, S.F.** Influence of the Welding Sequence on Residual Stress and Distortion of Fillet Welded Structures *Marine Structures* 46 2016: pp. 30 – 55. https://doi.org/10.1016/j.marstruc.2015.12.001
22. **Asuero, A.G., Sayago, A., González, A.G.** The Correlation Coefficient: An Overview *Critical Reviews in Analytical Chemistry* 36 (1) 2006: pp. 41 – 59. https://doi.org/10.1080/10408340500526766
23. **Pagani, E.** Tricks for Maximizing Collective Utility Functions *Working Papers No. 2* 2013: pp. 1 – 16.
24. **Perić, M., Seleš, K., Tonković, Z., Lovrenić-Jugović, M.** Numerical Simulation of Welding Distortions in Large Structures with a Simplified Engineering Approach *Open Physics* 17 (1) 2019: pp. 719 – 730. https://doi.org/10.1515/phys-2019-0076